SCIENCE CHINA
Chemistry

•COMMUNICATIONS•

July 2023 Vol.66 No.7: 1982–1988
https://doi.org/10.1007/s11426-023-1638-0

Weakly-solvating electrolytes enable ultralow-temperature (−80 °C) and high-power CF_x/Li primary batteries

Hao-Jie Liang[1†], Meng-Yuan Su[2†], Xin-Xin Zhao[2], Zhen-Yi Gu[1], Jia-Lin Yang[1], Wei Guo[3], Zhi-Ming Liu[4], Jing-Ping Zhang[2] & Xing-Long Wu[1*]

[1]*MOE Key Laboratory for UV Light-Emitting Materials and Technology, Northeast Normal University, Changchun 130024, China;*
[2]*Department of Chemistry, Northeast Normal University, Changchun 130024, China;*
[3]*Key Laboratory of Organo-Pharmaceutical Chemistry of Jiangxi Province, Gannan Normal University, Gan Zhou 341000, China;*
[4]*Qingdao University of Science and Technology, Qingdao 260061, China*

Received February 2, 2023; accepted May 11, 2023; published online May 29, 2023

Fluorinated carbons (CF_x)/Li primary batteries with high theoretical energy density have been applied as indispensable energy storage devices with no need for rechargeability, yet plagued by poor rate capability and narrow temperature adaptability in actual scenarios. Herein, benefiting from precise solvation engineering for synergistic coordination of anions and low-affinity solvents, the optimized cyclic ether-based electrolyte is elaborated to significantly facilitate overall reaction dynamics closely correlated to lower desolvation barrier. As a result, the excellent rate (15 C, 650 mAh g^{-1}) at room-temperature and ultra-low-temperature performance dropping to −80 °C (495 mAh g^{-1} at average output voltage of 2.11 V) is delivered by the end of 1.5 V cut-off voltage, far superior to other organic liquid electrolytes. Furthermore, the CF_x/Li cell employing the high-loading electrode (18–22 mg cm^{-2}) still yields 1,683 and 1,395 Wh kg^{-1} in the case of −40 °C and −60 °C, respectively. In short, the novel design strategy for cyclic ethers as basic solvents is proposed to enable the CF_x/Li battery with superb subzero performances, which shows great potential in practical application for extreme environments.

CF_x/Li primary batteries, solvation engineering, desolvation barrier, ultra-low temperature

Citation: Liang HJ, Su MY, Zhao XX, Gu ZY, Yang JL, Guo W, Liu ZM, Zhang JP, Wu XL. Weakly-solvating electrolytes enable ultralow-temperature (−80 °C) and high-power CF_x/Li primary batteries. *Sci China Chem*, 2023, 66: 1982–1988, https://doi.org/10.1007/s11426-023-1638-0

The development of society deserves energy-storage devices provided with high energy/power density and environmental adaptability [1]. The fluorinated carbons/lithium (CF_x/Li) primary batteries as one of the most prominent candidates have been universally used in medical, military, aerospace, and defense fields without rechargeability, owning to the higher theoretical energy density exceeding 2,100 Wh kg^{-1} (x=1), excellent safety, and low self-discharge rate [2–8]. However, the practical application scenarios are severely restricted by reason of sluggish reaction kinetics together with increasing cell resistance under extreme environments caused by intrinsically low electronic conductivity of CF_x/LiF and lack of suitable electrolytes [9]. In contrast to complicated and high-cost methods devoted to modifying CF_x materials, targeted electrolyte engineering is in urgent demand for an effective approach to promote rate and low-temperature performance [10–15].

The systematic researches on electrolytes trace back to the evolution of reaction mechanism for CF_x/Li batteries in the eighties of last century [16]. It is noteworthy that the electrolyte acting as the ionic mediator equally takes part in the discharge reaction [17]. The solvent molecules have been found to participate in the conversion-type reaction and af-

†These authors contributed equally to this work.
*Corresponding author (email: xinglong@nenu.edu.cn)

fect the electrochemical performance with the co-intercalation of the solvated Li^+ into CF_x layers as a ternary graphite intercalation compound (t-GIC) intermediate phase formed in a two-stage reaction pathway ($C_xF+Li+zS \rightarrow C_x(Li^+ \cdot zS)F^- \rightarrow xC+LiF+zS$, S termed as solvent molecule) where the specific desolvation process is divided into two parts happening before the co-intercalation of t-GIC and before the formation of LiF [16,18,19]. As a result, the researchers found that the discharge voltage plateau is enhanced by selecting strong coordination solvent with better electron-donicity [20]. In addition, the anions derived from salts are also proved to exert an effect on the performance [21].

Except for the effect of electrolyte components on reaction thermodynamics, the solvated microstructure accompanied with the solvation/desolvation process is also closely relevant to the dynamics [18]. From the perspective of temperature sensitivity of solvation interaction, different from the slight barrier distinction distributed in the semblable order of magnitude at room temperature, the dramatically inhibited Li^+ desolvation process as the rate-limiting step has been verified to be crucial for the kinetic behavior at low temperature [22,23]. Therefore, how to significantly reduce the desolvation energies of Li^+ is the key to formulate low-temperature electrolytes with ensuring sufficient ionic conductivity as a precondition [24,25]. By far, the massive efforts have been devoted to prioritizing low freezing point/viscosity solvents to optimize the electrolyte composition ensuring the ion transport in liquid phase. The commercial electrolyte formula consisting of 1 mol L^{-1} $LiBF_4$ dissolved in propylene carbonate (PC)/1,2-dimethoxyethane (DME) show the improved performance at −40 °C compared with carbonate-based electrolytes [26]. Moreover, the co-solvents (carboxylic ester (methyl butyrate, MB and isobutyl acetate) [9,27], fluorinated ether [28], and acetonitrile [29]), functional additives (tris(1,1,1,3,3,3-hexafluoroisopropyl) borate [30], BF_3 [31], and tris(2,2,2-trifluoroethyl) borate) [26], and novel liquefied gas electrolytes were recently reported [32]. However, the universally lower average operational voltages and narrow capacity are delivered with ever-increasing desolvation energies below −40 °C for the lack of precise control of solvation structure [23]. Similarly, to improve the fast-discharge capability at a high-rate current, the low desolvation kinetics needs to be endowed as well [33].

Herein, benefiting from the precise Li^+-coordinated regulation by the integration of low-affinity solvents with anions, the weakly solvating cyclic ether-based electrolyte is firstly introduced to significantly decrease desolvation activation energies and facilitate reaction kinetics, achieving superior rate-capability and ultralow temperature adaptability up to −80 °C. Discharged until 1.5 V cut-off voltage, the assembled CF_x/Li batteries yield 723, 652, and 495 mAh g^{-1} with average output voltages of 2.26, 2.22, and 2.11 V at −40 °C, −60 °C, and −80 °C, respectively, which is the best performance among current organic liquid electrolytes to the best of our knowledge. The capacity retention approaching 82% is produced at a high rate of 15 C (12 A g^{-1}). When increasing the loading of the active substance to 18–22 mg cm^{-2}, the energy densities of 1,683, 1,395, and 213 Wh kg^{-1} are still displayed at −40 °C, −60 °C and −80 °C, respectively. In a word, we propose a promising approach to design low-temperature electrolytes and expand the range of solvent options, promoting their application research on CF_x/Li primary batteries under cold environment.

The cyclic ethers as low-temperature solvents are known for inherent advantage in terms of physicochemical properties and weak affinity of Li^+ [34]. As shown in Figure 1a, the freezing points of representative DOL and THF are around −100 °C, far lower linear ethers (DME), cyclic carbonates (PC), and carboxylic ester (MB). And the lower viscosity renders the fluidity of liquid, which is essential for the employment at ultra-low temperature. The binding energies of different Li^+–solvent complexes are calculated by density functional theory (DFT). It can be seen that cyclic ethers show the weakest affinity of Li^+, obviously reducing the resistance to separation and assure the reductive stability with Li metal. In general, the solvent of the weak interaction with Li^+ has low dielectric constants, resulting in the weak solubility of lithium salts. Exceptionally, the THF is capable of dissociating lithium salts ($LiPF_6$, particularly for $LiBF_4$ widely used in low-temperature primary battery) effectively ascribed to favorable dielectric constants and acceptable Lewis basicity (donor number). Therefore, the optimized cyclic ether-based electrolyte (simplified as CEE) recipe is formulated by dissolving 1 mol L^{-1} $LiBF_4$ in the cyclic ether-based mixture of DOL and THF with 1:4 volume ratio. The commercial electrolyte (simplified as COE), 1 mol L^{-1} $LiBF_4$ in PC/DME (1:1 volume ratio), is prepared as athe contrast. Figure 1b shows temperature-dependent ionic conductivities of the formulated CEE and COE in the range from −80 °C to −40 °C. Compared with COE sharply minimized at −60 °C, the CEE possess-based ionic conductivity of 1.52, 1.35, and 1.29 mS cm^{-1} at −40 °C, −60 °C, and -80 ˚C, respectively, satisfying the corresponding criterion reported for low-temperature electrolytes in literature. Raman spectra are exhibited in Figure 1c to detect the formed solvation characteristics of COE and CEE. It is observed for COE that the DME and PC are jointly involved in solvation structure along with obvious blue shift of C–O–C (from pristine 848 to 869 cm^{-1}) and C=O (from pristine 1,781 to 1,792 cm^{-1}) stretching modes [35]. And the BF_4^- also participates in the solvation shell with the dominant formation of contact ion pairs (CIPs, BF_4^- coordinating with one Li ion) [21]. In addition, the slight blue shifts of C–O–C stretching vibration peaks assigned to THF and DOL also occur for CEE, indicating that the solvents exert the weak affinity of Li^+,

(a)

Solvent	Freezing point (°C)	Viscosity (mPa s)	Dielectric constant	Binding energy of Li^+-solvent complex (kJ mol^{-1})
PC	−48.8	2.53	64.9	−215.2
MB	−85.8	0.541	5.48	−207.3
DME	−58	0.45	5.5	−265.1
DOL	−97.2	0.6	6.74	−162.7
THF	−108.5	0.46	7.58	−189.7

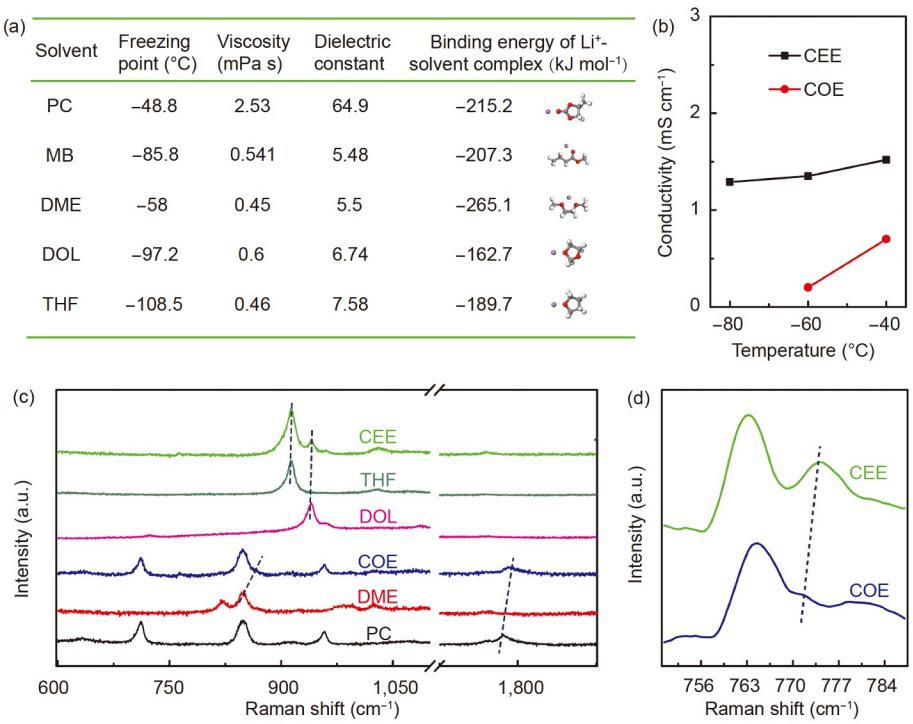

Figure 1 The characteristics of formulated electrolytes. (a) Summary to intrinsic physical properties of solvents and different binding energies with Li^+. (b) The ionic conductivities at different measured temperatures. (c) Raman spectra of solvents, COE and CEE. (d) The locally amplified Raman spectra for $LiBF_4$ salt as for B–F stretching (color online).

which contributes to the participation of anions in solvated coordination on the other hand [25]. As observed in Figure 1d, the obvious blue shift of the B–F stretching peak induced by solvated BF_4^- further demonstrates that more anions participate in the solvation sheath to form CIPs and more aggregate clusters (AGGs, BF_4^- coordinating with two/more Li ions) [36].

To further probe more specific solvation structure, the classical molecular dynamics (MD) simulations regarding COE and CEE are adopted by constructing electrolyte models at 25 °C and −40 °C with the ternary $LiBF_4$/PC/DME mixture (10 $LiBF_4$+58 PC+48 DME) and $LiBF_4$/THF/DOL mixture (10 $LiBF_4$+98 THF+28 DOL) based on conversion salt/solvent molar ratios [37]. The resulting snapshots are shown in Figure 2a, b and Figure S1a, b. The simulated results at 25 °C are shown in Figure S1c, d, consistent with above-mentioned Raman spectra. And the solvation effect is remarkably strengthened as the temperature drops. For COE at −40 °C, the radial distribution functions (RDFs) and related coordination number (Figure 2c) manifest Li^+ is coordinated with average 1.81 DME oxygens, 2.16 PC oxygens, and 1.08 BF_4^- borons at on average 1.97, 1.97, and 3.05 Å, and the increased share of DME and tight solvation structure compared with the case at 25 °C. By contrast, the weakened solvent coordination is observed in CEE together with an average 2.48 THF oxygens and 0.18 DOL oxygens at on average 1.89 and 1.93 Å, while the coordinating capability of anion in the solvation sheath significantly increases with the formation of CIP and AGG accompanied with an average coordination number of 1.63 BF_4^- borons at on average 3.03 Å, generating the compact configuration with the synergistic coordination of tight anions and alienated solvents (Figure 2d). The representative enlarged solvation microstructures (Figure 2e, f) consisting of Li^+–2PC–DME–BF_4^- and Li^+–3THF–DOL–BF_4^- are selected as the same CIP standard from the optimized −40 °C MD result to quantitatively study the discrepancy of desolvation activation energies between COE and CEE. The weakly-solvating structure is elaborated with the lower desolvation energy (5.12 eV) of CEE at −40 °C, far below that of COE (6.40 eV), corroborating that CEE possesses facile low-temperature dynamics compared with COE (Figure S2).

The electrochemical performance is tested in the CF_x/Li cell discharged to cut-off voltage of 1.5 V with the formulated electrolytes to prove evident superiority of CEE to COE at the low temperature and high rate (Figure S3). The galvanostatic discharge profiles with different rates at 25 °C are shown in Figure 3a. The CF_x/Li cell using CEE shows a specific capacity of 793 mAh g^{-1} with the discharge plateau about 2.57 V *versus* Li/Li^+ at 0.1 C (hence 1 C is standardized as 800 mA g^{-1} in this paper), slightly less than that using COE with 820 mAh g^{-1}. However, along with the in-

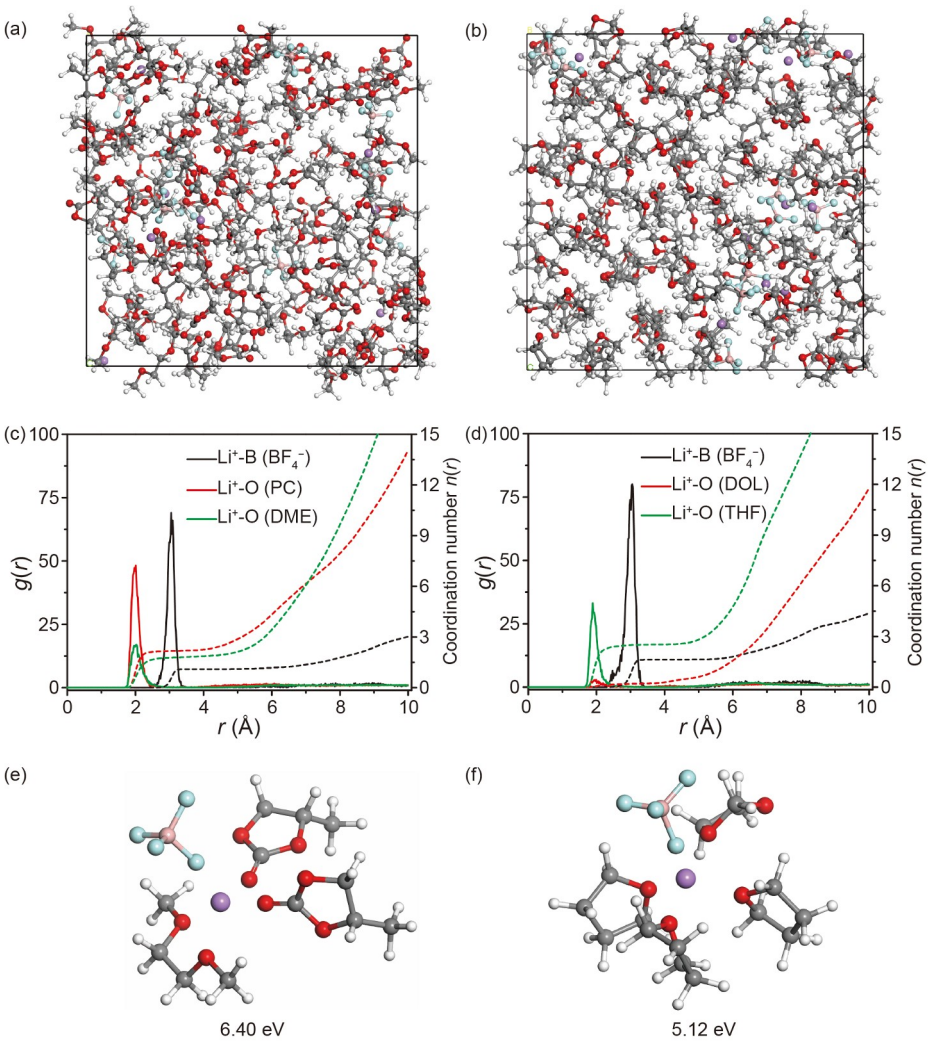

Figure 2 The MD simulations and quantitative calculation of desolvation energies regarding COE and CEE. Snapshot: Li^+ RDFs and related coordination numbers conducted from MD simulations of (a, c) COE and (b, d) CEE at −40 °C. The representative solvation structures of CIPs from MD simulations and the relevant desolvation energies of (e) COE and (f) CEE (color online).

creasement of current density from 0.2 C to 10 C, the cell still performs discharge capacities of 776, 775, 773, 772, 760, and 758 mAh g^{-1} enabled by the average output voltage of 2.51, 2.48, 2.41, 2.38, 2.32, 2.16, and 2.10 V, respectively. Especially at the high rate of 15 C, the discharge capacity of 650 mAh g^{-1} corresponding to 82% capacity retention is maintained with the average output voltage of 1.83 V, in comparison to less than 77 % capacity at 5 C in COE. When tested at −40 °C, the excellent performance (723, 690, 653, 592, and 498 mAh g^{-1} with the discharge plateaux about 2.3, 2.26, 2.16, 2.06, and 1.92 V) is yielded at 0.1, 0.2, 0.5, 1, and 2 C, respectively (Figure 3b). Moreover, Figure 3c also shows equally excellent capacities of 652, 622, 603, and 424 mAh g^{-1} provided with the average output voltage of 2.22, 2.18, 2.13, and 1.96 V at 0.03, 0.05, 0.1, and 0.5 C at −60 °C, respectively. Even expanded to almost unexplored −80 °C, the discharge capacity of 495 mAh g^{-1} is still displayed at 10 mA g^{-1} with the discharge plateau about 2.13 V, corresponding to the energy density of 1,044 Wh kg^{-1} (average output voltage of 2.11 V), bare of the preceding reports in such cold temperature (Figure 3d) [32]. By contrast, the COE only delivers 421 and 233 mAh g^{-1} capacities at −40 °C (0.1 and 0.5 C) and almost no remaining capacity at −60 °C. To further prove the potential of CEE for practical applications, the high-loading CF_x electrodes with 18–22 mg cm^{-2} are assembled with CEE, showing 781, 771, 717, 588 mAh g^{-1} with the average output voltage of 2.50, 2.45, 2.37, and 2.25 V at 0.02, 0.05, 0.1, and 0.2 C, obviously superior to COE (557 mAh g^{-1} at 0.1 C) (Figure 3e, Figure S4). Even in the case of −40 °C, −60 °C and −80 °C, the CF_x/Li cell still exhibits energy densities of 1,683, 1,395, and 213 Wh kg^{-1} enabled by 726, and 633, and 110 mAh g^{-1}, respectively (Figure 3e, Figures S5, S6). By contrast, the inferior performance is shown with high-loading electrodes with COE. In conclusion, the CEE enables Li/CF_x cells with the highest energy density at ultra-low temperatures com-

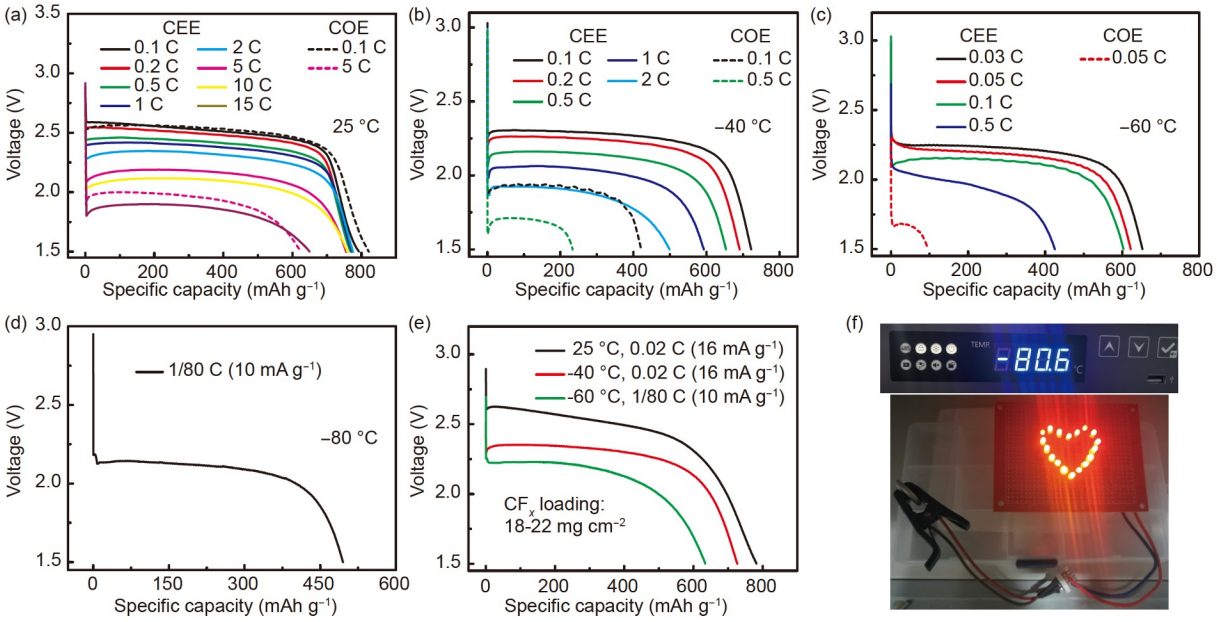

Figure 3 The electrochemical properties of CF_x/Li cells with CEE and COE. (a) Discharge curves of CF_x/Li primary cells using COE and CEE under different current densities from 0.1 to 15 C at room temperature. Low-temperature performance ranging from (b) −40 °C, (c) −60 °C to (d) −80 °C at different rates. (e) Discharge profiles at 25 °C, −40 °C, −60 °C, −80 °C realized by high-loading CF_x. (f) Actual operating image with LED lamps at −80 °C (color online).

pared with other reported organic liquid electrolytes, the superior performance, cost-effectiveness and practical scalability to further boost the development of next-generation primary batteries in cold environments [26,27]. Finally, the fabricated button cell with CEE succeeds in lighting up LED lamps at −80 °C, indicative of practical ultralow-temperature adaptability (Figure 3f).

To further comprehend the reason for the outstanding performance delivered by CEE, the electrochemical impedance spectroscopy (EIS) is obtained before the discharge at 25 °C and −40 °C to study the kinetic properties of CF_x/Li cells using COE and CEE (Figure 4a, b). When the temperature decreases from 25 °C to −40 °C, the overall impedance rises rapidly, which indicates that dynamic processes are severely limited by certain temperature-dependent modules. In addition, it is noteworthy that the cells using CEE retain almost one-eighteenth of total impedance from counterparts using COE at −40 °C, well explaining the excellent electrochemical performance. To identify the underlying determinants, the EIS spectrum is fitted with an equivalent circuit model (Figure S7) with the bulk resistance of electrolyte itself (R_b), Li^+ transport resistance through the solid electrolyte interphase (SEI, R_{SEI}), and Li^+ desolvation also known as charge transfer resistance (R_{ct}) [9]. The integration of the slightly increased R_b and R_{SEI} identified as minor factors, the dominant proportion and significant increasement of R_{ct} dependent on temperature reduction at −40 °C confirm the desolvation process of Li^+ as the rate-limiting step to determine the low-temperature performance of CF_x/Li batteries, in accordance with previous studies. Therefore, the significantly reduced R_{ct}, namely desolvation energy, is the root cause for elevating low-temperature performance in CEE. The impacts of electrolytes on the CF_x electrode and the interface are correlated to scanning electron microscopy (SEM), high-resolution transmission electron microscopy (HRTEM), and X-ray photoelectron spectroscopy (XPS). As shown in Figure S8, the undersized LiF grain sizes and lamellar-exfoliated carbon products are clearly observed in CEE, illustrating the complete involvement in the discharge reaction at −40 °C [38]. By contrast, the bulk CF_x residues and relatively integrated structure without the fracture obviously exist owning to the poor reactivity. The thin and dense interfacial films formed on the cathode surface in CEE are characterized with favorable structural integrity to ensure the solvated ion diffusion through SEI (Figure 4c). The XPS is performed on the fully discharged CF_x electrode at −40 °C to investigate the chemical composition of SEI (Figure 4d). The C–C and C–F bonds are assigned to the intrinsic structure of pristine CF_x materials, while C–O represent the composition of formed film [21]. It can be seen from C 1s and F 1s spectra that the C–F peak located at 290.4 eV relatively decreases accompanied with C–O bonds appearing at 285.8 eV when discharged to 1.5 V in CEE and COE, confirming the similarity of interfacial chemistry in ether-based electrolytes. The higher Li–F peak at 686.1 eV is observed in CEE due to a thorough CF_x conversion from C–F compared with COE (Figure S9). On the basis of the above analyses, it is concluded that the interface chemistry exerts unconspicuous effects on the low-temperature performance of the battery. In short, as depicted in Figure 5, in light of the

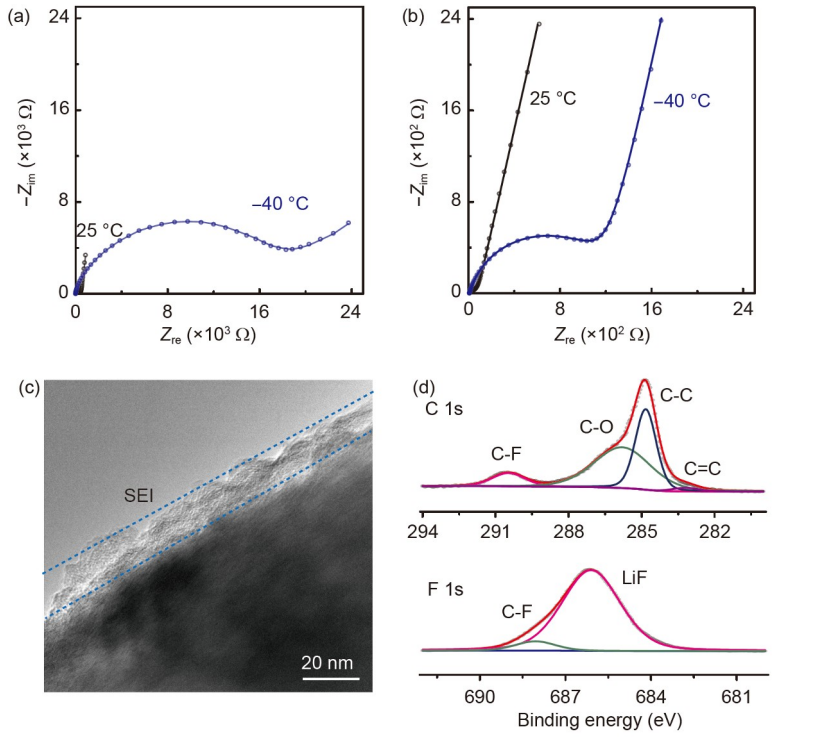

Figure 4 Nyquist plots and interfacial characterizations. The EIS spectra of CF_x/Li cells using (a) COE and (b) CEE before the discharge at 25 °C and −40 °C. The SEI analyses by (c) HRTEM and (d) high-resolution XPS C 1s and F 1s assignments when fully discharged at −40 °C in CEE (color online).

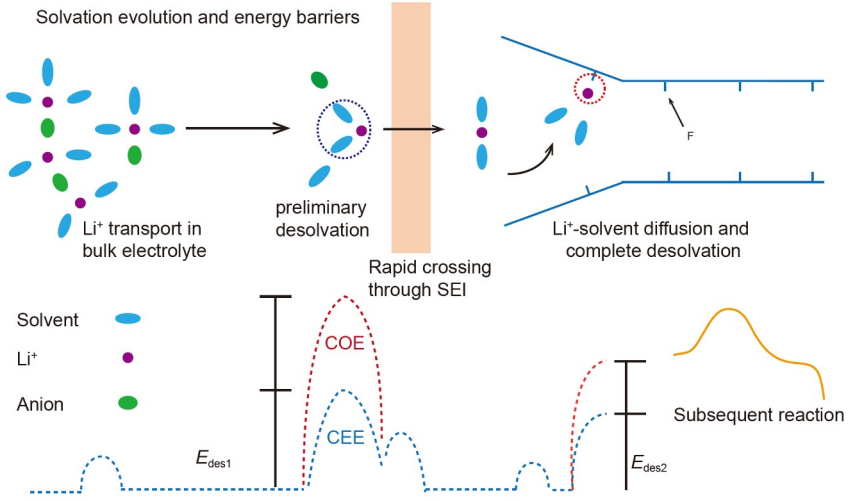

Figure 5 The schematic diagram of solvation evolution and relevant energy barriers presented in each process (color online).

involvement of solvents in the specific reaction of the CF_x/Li cell differing from merely acting as the ionic mediator in traditional rechargeable batteries, the focus should be on two-sided effects of desolvation process in the CF_x/Li cell on the interfacial ion-transport efficiency and reaction dynamics. The CEE significantly reduces the desolvation energy barrier consisting of E_{des1} and E_{des2}, achieving faster integrated dynamics than COE at the low temperature. Therefore, the solvent substitution of carbonates with cyclic ethers is beneficial to exploit electrolytes at ultra-low temperature.

In this work, by designing the weakly-solvating structure involving the synergistic coordination of tight anions and alienated solvents, the optimized CEE is proved to significantly decrease desolvation activation energies and facilitate whole dynamics, achieving the superior rate-capability and ultralow-temperature adaptability. The CF_x/Li batteries in CEE show 776, 773, 758, and 650 mAh g^{-1} at

0.1, 0.5, 10, and 15 C at 25 °C. When the temperature drops to −40 °C, −60 °C, and −80 °C, the capacities of 723, 652, and 495 mAh g^{-1} are maintained with average output voltages of 2.26, 2.22, and 2.11 V, corresponding to energy densities of 1,634, 1,447 and 1,044 Wh kg^{-1}, respectively. And the voltage plateaux exceeding 2 V are yielded with 2.3, 2.24, and 2.13 V at −40 °C, −60 °C, and −80 °C, much higher than other reports. To further testify the potential for practical applications, the CF_x loading is increased to 18–22 mg cm^{-2}. The assembled CF_x/Li cells also show energy densities of 1,683 and 1,395 Wh kg^{-1} at −40 °C and −60 °C. In brief, we provide a powerful method for the electrolyte modification with cost-effectiveness and practical scalability, which has unexploited the application value and favorable exploitation foreground for ultralow-temperature primary batteries.

Acknowledgements This work is financially supported from the Natural Science Foundation of Jilin Province (20220508141RC).

Conflict of interest The authors declare no conflict of interest.

Supporting information The supporting information is available online at chem.scichina.com and link.springer.com/journal/11426. The supporting materials are published as submitted, without typesetting or editing. The responsibility for scientific accuracy and content remains entirely with the authors.

1 Xie F, Xu Z, Guo Z, Lu Y, Chen L, Titirici MM, Hu YS. *Sci China Chem*, 2021, 64: 1679–1692
2 Sayahpour B, Hirsh H, Bai S, Schorr NB, Lambert TN, Mayer M, Bao W, Cheng D, Zhang M, Leung K, Harrison KL, Li W, Meng YS. *Adv Energy Mater*, 2022, 12: 2103196
3 Zhang SS, Foster D, Read J. *J Power Sources*, 2009, 188: 601–605
4 Sharma N, Dubois M, Guérin K, Pischedda V, Radescu S. *Energy Tech*, 2021, 9: 2000605
5 Zhou CC, Su Z, Gao XL, Cao R, Yang SC, Liu XH. *Rare Met*, 2022, 41: 14–20
6 Sun J, Wang T, Gao Y, Pan Z, Hu R, Wang J. *InfoMat*, 2022, 4: e12359
7 Yang Q, Jiang N, Shao Y, Zhang Y, Zhao X, Zeng Y, Qiu J. *Sci China Chem*, 2022, 65: 2351–2368
8 He Y, Liu M, Chen S, Zhang J. *Sci China Chem*, 2022, 65: 391–398
9 Xue W, Qin T, Li Q, Zan M, Yu X, Li H. *Energy Storage Mater*, 2022, 50: 598–605
10 Fulvio PF, Brown SS, Adcock J, Mayes RT, Guo B, Sun XG, Mahurin SM, Veith GM, Dai S. *Chem Mater*, 2011, 23: 4420–4427
11 Li Y, Wu X, Liu C, Wang S, Zhou P, Zhou T, Miao Z, Xing W, Zhuo S, Zhou J. *J Mater Chem A*, 2019, 7: 7128–7137
12 Luo Z, Wang X, Chen D, Chang Q, Xie S, Ma Z, Lei W, Pan J, Pan Y, Huang J. *ACS Appl Mater Interfaces*, 2021, 13: 18809–18820
13 Peng C, Li Y, Yao F, Fu H, Zhou R, Feng Y, Feng W. *Carbon*, 2019, 153: 783–791
14 Whitacre J, Yazami R, Hamwi A, Smart MC, Bennett W, Surya Prakash GK, Miller T, Bugga R. *J Power Sources*, 2006, 160: 577–584
15 Huang J, Li F, Wu M, Wang H, Qi S, Jiang G, Li X, Ma J. *Sci China Chem*, 2022, 65: 840–857
16 Watanabe N, Nakajima T, Hagiwara R. *J Power Sources*, 1987, 20: 87–92
17 Leung K, Schorr NB, Mayer M, Lambert TN, Meng YS, Harrison KL. *Chem Mater*, 2021, 33: 1760–1770
18 Jiang J, Ji H, Chen P, Ouyang C, Niu X, Li H, Wang L. *J Power Sources*, 2022, 527: 231193
19 Watanabe N, Hagiwara R, Nakajima T, Touhara H, Ueno K. *Electrochim Acta*, 1982, 27: 1615–1619
20 Fu A, Xiao Y, Jian J, Huang L, Tang C, Chen X, Zou Y, Wang J, Yang Y, Zheng J. *ACS Appl Mater Interfaces*, 2021, 13: 57470–57480
21 Wang X, Song Z, Wu H, Yu H, Feng W, Armand M, Huang X, Zhou Z, Zhang H. *Angew Chem Int Ed*, 2022, 61: e202211623
22 Ma T, Ni Y, Wang Q, Zhang W, Jin S, Zheng S, Yang X, Hou Y, Tao Z, Chen J. *Angew Chem Int Ed*, 2022, 61: e202207927
23 Zhang N, Deng T, Zhang S, Wang C, Chen L, Wang C, Fan X. *Adv Mater*, 2022, 34: 2107899
24 Hubble D, Brown DE, Zhao Y, Fang C, Lau J, McCloskey BD, Liu G. *Energy Environ Sci*, 2022, 15: 550–578
25 Jin CB, Yao N, Xiao Y, Xie J, Li Z, Chen X, Li BQ, Zhang XQ, Huang JQ, Zhang Q. *Adv Mater*, 2023, 35: 2208340
26 Whitacre JF, West WC, Smart MC, Yazami R, Prakash GKS, Hamwi A, Ratnakumar BV. *Electrochem Solid-State Lett*, 2007, 10: A166
27 Fang Z, Yang Y, Zheng T, Wang N, Wang C, Dong X, Wang Y, Xia Y. *Energy Storage Mater*, 2021, 42: 477–483
28 Ban J, Jiao X, Feng Y, Xue J, He C, Song J. *ACS Appl Energy Mater*, 2021, 4: 3777–3784
29 Zhang SS, Foster D, Read J. *J Power Sources*, 2009, 188: 532–537
30 Nagasubramanian G, Sanchez B. *J Power Sources*, 2007, 165: 630–634
31 Li Q, Xue W, Sun X, Yu X, Li H, Chen L. *Energy Storage Mater*, 2021, 38: 482–488
32 Yin Y, Holoubek J, Liu A, Sayahpour B, Raghavendran G, Cai G, Han B, Mayer M, Schorr NB, Lambert TN, Harrison KL, Li W, Chen Z, Meng YS. *Adv Mater*, 2023, 35: 2207932
33 Sun C, Ji X, Weng S, Li R, Huang X, Zhu C, Xiao X, Deng T, Fan L, Chen L, Wang X, Wang C, Fan X. *Adv Mater*, 2022, 34: 2206020
34 Luo D, Li M, Zheng Y, Ma Q, Gao R, Zhang Z, Dou H, Wen G, Shui L, Yu A, Wang X, Chen Z. *Adv Sci*, 2021, 8: 2101051
35 Jiang LL, Yan C, Yao YX, Cai W, Huang JQ, Zhang Q. *Angew Chem Int Ed*, 2021, 60: 3402–3406
36 Liang HJ, Gu ZY, Zhao XX, Guo JZ, Yang JL, Li WH, Li B, Liu ZM, Sun ZH, Zhang JP, Wu XL. *Sci Bull*, 2022, 67: 1581–1588
37 Liang HJ, Gu ZY, Zhao XX, Guo JZ, Yang JL, Li WH, Li B, Liu ZM, Li WL, Wu XL. *Angew Chem Int Ed*, 2021, 60: 26837–26846
38 Long S, Chen F, Ding F, Han Y, Liu X, Xu Q. *J Phys Chem C*, 2019, 123: 28048–28057